MEASUREMENT OF VERY SLOW FLOWS IN ENVIRONMENTAL ENGINEERING

Thesis submitted

in fulfillment of the requirements for the degree of

Doctor of Philosophy

by Andrew Skinner

Faculty of Engineering, Computer and Mathematical Sciences

School of Civil, Environmental and Mining Engineering

The University of Adelaide, North Terrace Campus

South Australia

December 2009

Measurement of Very Slow Flows in Environmental Engineering

By: Andrew John Skinner

B.Tech., M.Eng. (Electronic Engineering), FIEAust., CPEng

Thesis submitted in fulfillment of the requirements for the degree of Doctor of Philosophy

LIBRARY COPY after examination

Faculty of Engineering, Computer and Mathematical Sciences
School of Civil Environmental and Mining Engineering
The University of Adelaide SA 5005 Australia

Correspondence to: -
Andrew Skinner
Engineering Director
Measurement Engineering Australia
41 Vine Street
PO Box 476
MAGILL, South Australia 5072
Telephone: +61 8 8332 9044
Facsimile: +61 8 8332 9577
Web: www.mea.com.au
Email: andrew.skinner@mea.com.au

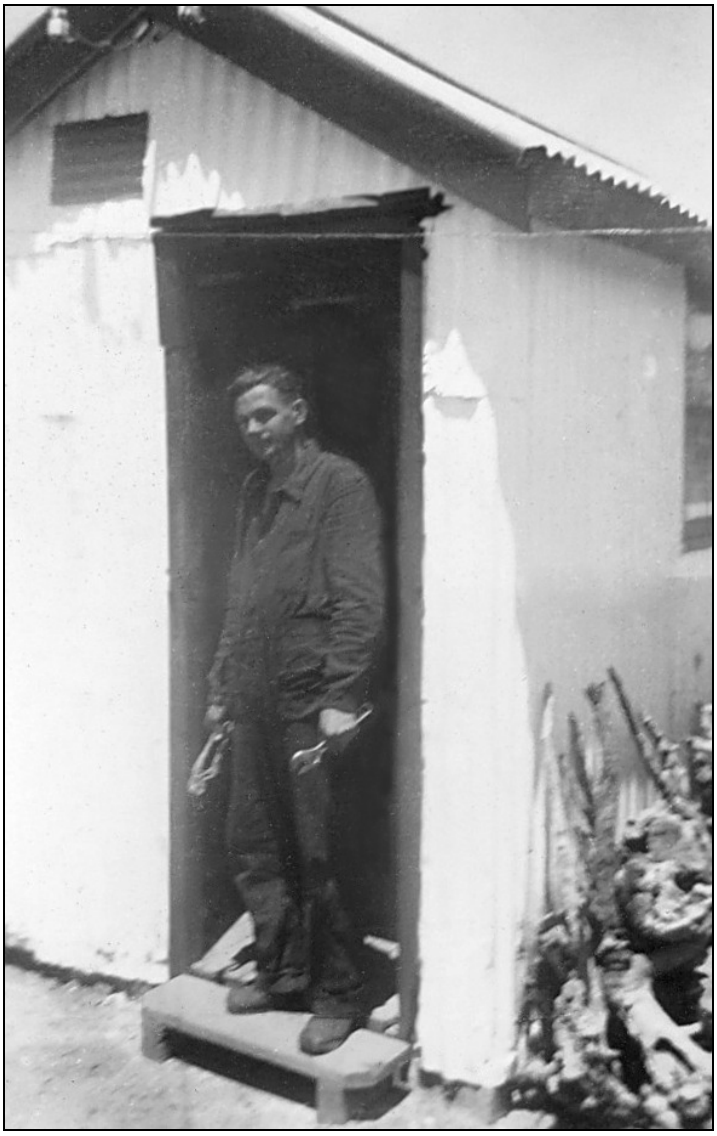

I dedicate this thesis to my father

John Francis Skinner

24th September 1923 – 3rd March 1983

who left school after Grade 7 to train in the hard school of engineering
in a country garage in the Western Australian wheat-belt town of Merredin.

He went on to build up a highly-regarded ‘custom engineering’ firm
capable of building specialist machines for industry and universities.

Sadly, he never lived to see his eldest son do the same in the field of
measurement engineering.

He left me the skill in my hands,
an imagination tuned for building gadgetry
and the sense that with hard work anything is possible.

Table of contents

MEASUREMENT OF VERY SLOW FLOWS IN ENVIRONMENTAL ENGINEERING..... I

TABLE OF CONTENTS IV

TABLE OF FIGURES.....VI

STATEMENT X

ACKNOWLEDGMENTS XI

ABSTRACT 1

CHAPTER 1. INTRODUCTION 5

CHAPTER 2. LITERATURE REVIEW 11

2.1 VERY SLOW FLOWS IN STRATIFIED LAKES 12
2.2 'RATE-OF-HEAT LOSS' FLOW METERS IN THE LITERATURE 14
2.2.1 Thermistor flow meters in the literature 15
2.2.2 The most basic thermistor flow meter 17
2.2.3 A simple temperature-compensated thermistor flow meter 17
2.2.4 An effective temperature-compensated thermistor flow meter 18
2.2.5 The LaBarbera and Vogel bridge 19
2.2.6 The Yang et al bridge 21
2.2.7 Digital thermistor bridge circuits 22
2.2.8 A transient response thermal flow sensor using intertwined PRTDs 23
2.2.9 A thermal gas-flow sensor using the digital oscillator technique 24
2.3 'TEMPERATURE RISE' OR 'THERMAL-FIELD DISTORTION' FLOW METERS 24
2.4 'TIME-OF-FLIGHT' THERMAL FLOW METERS 27
2.5 SUMMARY OF LITERATURE REVIEW FINDINGS 27
2.5.1 Thermistor resistance-temperature characteristics 27
2.5.2 The limitations of analog thermistor bridge flow meters 29
2.5.3 Thermistor flow meters for very slow flows 30
2.5.4 The problem of buoyancy in 'Rate of Heat Loss' sensors in open water bodies..... 32
2.5.5 Future directions from the literature 32

CHAPTER 3. USING SMART SENSOR STRINGS FOR CONTINUOUS MONITORING OF TEMPERATURE STRATIFICATION IN LARGE WATER BODIES..... 37

3.1 BACKGROUND 37
3.1.1 Development of a new SFVC ADC for sensors 38
3.1.2 The AD652 Synchronous Voltage-to-Frequency Converter: Product Description 39
3.1.3 An early SVFC thermistor ADC design 41
3.1.4 Development of an integrated temperature sensor 43
3.1.5 Use of 'standard curves' for linearizing non-linear sensor response 45
3.1.6 Improving sensor resolution and linearity 46

CHAPTER 4. AN AUTOMATIC SOIL PORE-WATER SALINITY SENSOR BASED ON A WETTING FRONT DETECTOR..... 51

4.1 BACKGROUND 51
4.1.1 Extending the ADC form to differential and AC excitation measurements..... 52

CHAPTER 5. A LOG-ANTILOG ANALOG CONTROL CIRCUIT FOR CONSTANT-POWER WARM-THERMISTOR SENSORS – APPLICATION TO PLANT WATER STATUS MEASUREMENT 59

5.1 BACKGROUND 59
5.1.1 Generating constant-power in a thermistor flow meter 61
5.1.2 The dual element heat source: thermilinear thermistor devices 63
5.1.3 The switched heat source 67
5.1.4 The dual current heat source 69
5.1.5 A switched bridge constant-power thermistor flow meter..... 70
5.1.6 An inverse square root circuit using analog hardware multipliers 76

5.1.7 Solving the inverse square-root function using digital multipliers ... *77*
5.1.8 A log-antilog inverse square-root circuit ... *78*

CHAPTER 6. EVALUATION OF A WARM-THERMISTOR FLOW SENSOR FOR USE IN AUTOMATIC SEEPAGE METERS ... **81**

6.1 BACKGROUND ... 81
6.1.1 Motivation for the development of a groundwater seepage meter ... *83*
6.1.2 Expanded Proof of the Varying Head Flow Controller ... *84*
6.1.3 'Plunging flow calibrator' control circuit ... *85*
6.1.4 The workbench… ... *88*
6.1.6 Transient flow calibration apparatus ... *89*
6.1.7 Flow transition from laminar to turbulent in the control pipe ... *91*

CHAPTER 7. A NULL-BUOYANCY THERMAL FLOW METER: APPLICATION TO THE MEASUREMENT OF THE HYDRAULIC CONDUCTIVITY OF SOILS ... **95**

7.1 BACKGROUND ... 95
7.1.1 Seepage meters and mechanical valves ... *95*
7.1.2 Buoyant plumes under downward flow conditions ... *97*
7.1.3 Flows in the landscape – 'hydraulic conductivity' and drainage meters ... *98*
7.1.4 Permeameters and the measurement of hydraulic conductivity ... *103*
7.1.5 Early results: problems with thermal stratification in the test rig ... *105*
7.1.6 Reducing thermal background temperatures ... *106*
7.1.7 Flow instability ... *107*
7.1.8 Plume stability ... *108*

CHAPTER 8. CONCLUSIONS AND FUTURE WORK ... **113**

CHAPTER 9. REFERENCES ... **119**

APPENDIX A: SELECTED FIELD DATA FROM TEMPERATURE SENSOR STRINGS ... **133**

APPENDIX B: BINARY LOGARITHMS FOR SOLVING THE STEINHART-HART EQUATION ... **139**

B1. Natural and binary logarithms ... *139*
B2. Deriving binary logarithms in a microcontroller ... *141*
B3. Approximating the binary logarithm with a simple arithmetic function ... *143*
B4. Solving for error terms in the Simple logarithm ... *144*
B5. Using a look-up table to reduce errors in the Simple logarithm ... *145*

APPENDIX C: THERMISTOR FORMULAE IN EXCEL SPREADSHEETS ... **149**

APPENDIX D: FAILURE OF MONOTONICITY IN THE ADC ... **151**

APPENDIX E: SAP FLOW BIBLIOGRAPHY ... **155**

Table of Figures

Figure 1 A simple constant-temperature hot wire/hot film anemometer, using an adjustable resistance to force a constant temperature onto the hot wire as described by Lomas (1986) and reproduced from Sheldrake (1995). Setting the variable resistance R_3 to a particular value forces the control loop to adjust the bridge voltage to impress a voltage across the hot-wire R_W, thus raising it to a constant temperature as it dissipates power. The bridge voltage E is the output signal, and varies as the fluid flow rate changes the rate-of-heat loss from the sensor element. 15
Figure 2 The simplest possible method of creating a warm thermistor flow meter, adapted from Molina, Victoria and Ibanez (1994). The voltage regulator impresses a DC voltage across the thermistor and the ammeter measures the current flow to ground as a flow-dependent signal. This method is dependent upon isothermal fluid temperature. 17
Figure 3 The Vogel (1969) warm thermistor flow meter 18
Figure 4 The Riedl and Machan (1972) Bridge Flowmeter. These early flow-monitoring bridge circuits were always in self-heating mode, and were unable to report on the temperature of either the water or the heated thermistor. Instead, their output was proportional to power dissipated by the self-heated thermistor. R_1=100Ω (adjustable), *R2*=1500Ω, *R3*=1200Ω, *T1*=100Ω thermistor, *T2*=1000Ω thermistor, *T1*=3000Ω thermistor at 25°C 19
Figure 5 The LaBarbera and Vogel (1976) bridge. A and B are the flow meter with voltage-to-frequency converter C and frequency-to-voltage converter D 20
Figure 6 The active-bridge flowmeter of Yang, Kummel and Soeberg (1988). R_m is the measurement thermistor and R_r is the reference thermistor 21
Figure 7 Pulsed thermistor bridge of Briggs-Smith and Piscitelli (1981) 23
Figure 8 Pulsed double-PRTD thermal flow meter of Sonnenschmidt and Vaneslow (1996). The double PT100 on the left has dimensions in millimetres. The wires are two intertwined spirals of the same diameter. 24
Figure 9 Industrial thermal flow meter of the type described by Baker (1995) 25
Figure 10 Thomas flow meter, with a heating element inside the pipe and thermocouples used to measure the induced temperature gradient. From Baker (1995) 25
Figure 11 The Laub flow meter placed the heating and sensor coils on the outside of the pipe for safety reasons. From Baker (1995) 25
Figure 12 Monolithic flow sensor of Yang and Soeberg (1992) – circuit and physical layouts – operating in transit-time flow mode 26
Figure 13 Resistance versus temperature response of a 1kΩ@25°C NTC thermistor measured with a 10μA excitation current 28
Figure 14 Error curves for the Rield-Machan Bridge over the limited temperature range of 5°C to 35°C for a mixture of commercial thermistor values *T1*, *T2* and *T3* with optimal fixed resistor values in *R1*, *R2* and *R3*. 29
Figure 15 Lewis (on the left) of the University of Adelaide installing an early raft-based stratification system in the Myponga Reservoir in South Australia. The multi-channel ADC electronics is installed in the enclosure at the rear of the raft. The multiple individual thermistors can be seen hanging over the front of the raft (white cables). 38
Figure 16 The AD652 Monolithic Synchronous Voltage-to-Frequency Converter used as the basis for the development of a new type of charge-balance ADC for environmental sensors. 40
Figure 17 An early SVFC thermistor ADC design. It is essentially a buffered voltage divider network followed by an active-low SVFC ADC formed by the integrator and comparator. V_{ref} is 1.23V and is derived ratiometrically from the LM2951 +5V regulator powering the thermistor divider, the comparator reference and the microcontroller. This design was used with remote thermistors on the end of a two-wire cable, often up to 30m from the ADC located in an enclosure on a surface raft as in Figure 15 or on a wooden pole driven into the sediment. 42
Figure 18 The remote thermistor of Figure 17 – submersed in the water column - was almost always operating at a different temperature to the electronics on the surface raft. This necessitated a separate measurement of the temperature of the ADC electronics. This was accomplished by this parallel ADC channel using a PNP diode-connected bipolar transistor as a temperature sensor. Small changes in the thermal voltage *kT/q* of the transistor's base-emitter voltage due to temperature fluctuations changed the input current of the ADC and hence its *count* output. This particular circuit gave rise to the possibility of a ground-referred thermistor in place of the PNP+R_{in} combination to measure temperature in an isothermal environment created by potting the ADC, thermistor, 5V regulator and microcontroller in close proximity. This reduced the difficulties in finding a convergent solution to the 7-parameter calibration associated with this separate temperature measurement solution. 42
Figure 19 Twenty-four sensor circuit boards are shown before being broken-out from the PCB panel form in which they are manufactured. They are shown linked by ribbon cable (top) to power, program and test them prior to encapsulation. They are then potted inside a threaded PVC tube with a cable-gland and

O-ring at each end. A heavy-walled adhesive heatshrink is then shrunk over the whole assembly to form a third level of waterproofing (bottom). 44
Figure 20. The 'count versus temperature' transfer functions of 26 randomly selected production sensors all follow the same basic curvature. Applying small offset and gain terms to each curve matches all sensors over the operating temperature range to within ±0.006°C, while effectively linearizing the calibration process. 45
Figure 21 A sensor string bundled together for two-point in-field calibration at the Torrens Lake in Adelaide South Australia 47
Figure 22 A 15-bit integrated thermistor temperature charge-balance ADC, published in IEEE Sensors in December 2006 48
Figure 23 An improved 16-bit integrated thermistor temperature charge-balance ADC, developed and field tested extensively after the original sensor was published in IEEE Sensors in December 2006. The separation of the op-amp and comparator (previously in a single 8-pin DIP package) resolved issues with 'flat-spots' in the temperature response curves due to internal IC feedback problems on the shared supply pin at harmonics of the SVFC clock, as explained in Appendix D 49
Figure 24 The Murray-Darling Basin in south-eastern Australia covers 14% of the county's total land area and is home to 11% of the Australian population. The Darling (2740km), Murray (2530km) and Murrumbidgee (1690km) are Australia's three longest rivers. 52
Figure 25 A 16-bit charge-balance ADC for platinum resistance temperature measurement. The bias current generator injects a 1mA current into the PRTD to offset the 1kΩ (0°C) baseline resistance of the PRTD; the ADC only responds to differential resistances above this value in the temperature range 0°C to 50°C 53
Figure 26 Drive circuitry for a four-electrode platinum electrical conductivity sensor. The EC sensor is driven by a 250 Hz push-pull square-wave via op-amp drivers U1A and U1B whose ground current is approximately equal to the AC current flowing through the conductivity cell. This conductivity current is rectified by the op-amp's output stage and is reflected through a 200:1 current-mirror into the input current side of the 16-bit charge-balance ADC. The LTC6078 micro-power dual op-amp was chosen for its very small quiescent current (an error term in the load current of the conductivity cell). 53
Figure 27 Two wetting-front detectors were installed at Oxford Landing in early 2009, with salinity sensors inserted in early July 2009 in the throats of the WFDs in place of the usual float rods. Continuing drought over the region has meant that insufficient rainfall has fallen to create a wetting front to provide field results in time for thesis publication. The 200-mm depth WFD is installed on the left, and the deeper 400-mm device on the right. Standard vacuum-based soil solute sampling tubes in the bottom left of the photo were installed at these same depths for comparison. The logging system is not shown. 54
Figure 28 Various commercial sap-flow systems (clockwise from top-left): Dynamax 'heat-balance' sap flow sensor, Greenspan 'heat pulse' sap flow sensors, sap flow measurements in large trees present extra challenges! Granier (thermal diffusion) sap flow sensors, physical model of the 'heat-balance' sap flow sensor, sap flow diagram for a tree, Granier sensors (centre). The white band around the tree in the photo on the bottom right-hand side is a 'dendrometer'; an instrument for the continuous monitoring of tree girth, and an indirect method of monitoring plant water status. 60
Figure 29 A thermilinear thermistor, consisting of a high-resistance thermistor thermally and electrically bonded to a low-resistance thermistor. 63
Figure 30 Constant power flow meter using a thermilinear element as a combined sense and heater 65
Figure 31 Block diagram of chopper-based single thermistor constant power heat source (power drive not shown) 67
Figure 32 Dual-current source constant-power thermistor heater. Details of the unity-gain buffer and synchronous demodulator are not shown. 69
Figure 33 Block diagram of the constant power thermistor bridge with inherent temperature measurement. The detail of the inverse square-root circuit is shown in Figure 34 71
Figure 34 Inverse square-root circuit using analog four-quadrant multipliers 77
Figure 35 Two reservoirs open to atmosphere have surface water heights of h_0 and h_3 above a nominal reference plane. The reservoirs are connected between heights h_1 and h_2 (in meters) by a pipe inside of which friction (viscous) forces result in an effective 'head loss' h_L. 84
Figure 36 'Plunging-probe' sensor calibration rig for generating very slow linear velocities for a warm-thermistor probe in an isothermal still water tank. A shaft-encoder [1] having a pulley wheel [2] of 500mm circumference, precision bearings and 1 mm resolution is driven by a DC-Micromotor [3] coupled to a precision all-metal spur gear head [4]. A beaded line [5] is balanced across this pulley wheel by lead counterweight [6] and the lead weight [7] on the stainless-steel shaft [8] carrying the thermistor. The motor raises and lowers the probe through the very still temperature-stable water body in the 20-litre Dewar vessel [9]. The output of the constant-power bridge circuit [10] is recorded by the 6½-digit Keithley K2000 recording multimeter [11]. Power supply and control circuits are not shown. The actual apparatus is shown in Figure 39. 86
Figure 37 Logic-based control circuit for the plunging probe calibration rig 87

Figure 38 The Keithley K2000 6½-digit recording multimeter (top-centre) is programmed from a customized computer program to carry out 1024 measurements at a rate of (typically) every second, measuring the output voltage of the double-bridge constant-power circuit. The close-up of the control and measurement circuit on the right-hand side shows the bread-boarded circuit of the schematic shown in Figure 37. It's not lovely, but it worked. 88
Figure 39 The Unidata shaft-encoder (left-top) monitors the vertical height of the probe balanced across its pulley wheel, which is driven directly by the motor-gearbox unit (right-centre). The Dewer flask sits below the shaft-encoder, and the beaded cable supporting the sensor probe passes through a small hole in the cork lid. 88
Figure 40 A 'single-sweep' seepage meter calibration system. This step-change variable head seepage meter calibrator uses a Hagen-Poiseuille flow controller. A 240-litre container [1] holds a 900-mm depth of well-mixed water at room temperature. The thermistor sensor located at level [4] is submerged by 50 mm when the 1000-mm high x 27.5 mm diameter bore vertical calibration sensor standpipe [2] and electronic control circuit [5] are in the top left-hand position. In this initial position, water in the vertical sensor standpipe is at the same level as the surface of the water in the main tank. When the instrument is plunged to the lower right-hand position, an instantaneous differential head pressure '*H*' is applied to opposite ends of the (coiled) Hagen-Poiseuille flow control pipe [3], which has a 5-mm bore and a length of 33m. *H* is the 'final height' of the step-change in water pressure. The electronics has been incorporated into the standpipe base in order to stabilize its temperature. 89
Figure 41 The seepage meter standpipe can just be seen above the water level in the tank at left. 90
Figure 42 The standpipe is shown in the water column, with the electronics below and the Hagen-Poiseuille flow control pipe to the left (the latter was later replaced by 33 m of wound plastic pipe to lower the Reynolds Number below turbulent flow speeds). Rather than step-change height, the method shown here purged the vertical standpipe using compressed air. Uncapping the top of the standpipe allowed water to flow back in with a first-order time-constant. 90
Figure 43 The seepage meter standpipe is shown with the 'level sensing' thermistors arranged in a logarithmic spacing up though its height. The level sensor spacings were chosen to allow roughly equal time intervals for the arrival of the water-air front at each heated sensor as the water level rose up through the column with decaying velocity, flowing in from the main tank through the flow control pipe on the left. 91
Figure 44 At high flow rates in the 'control pipe' (between 0 and 180 s into the run), flow becomes turbulent (high Reynolds Number) and limits flows in the vertical seepage meter standpipe, as shown by the deviation and oscillations of the flow sensor traces with respect to the expected (red) curve. 93
Figure 45 A bi-directional flow cell and electronics, configured as a differential flow detector, with the upward flow sensor being the master in the control loop, as set by the switch. The voltage across the upward flow sensor would be imposed across the slave thermistor in the downward flow section of the inverted tube. The difference in the thermistor currents – as detected by the instrumentation amplifier – would be the signal. 97
Figure 46 Maximum thermistor temperature occurs at a 1.35 mm/s downward flow that exactly balances the natural convective upward flow for a 40 mW heat output. This leads to a stagnation zone around the thermistor tip that results in maximum heating of the sensor under any flow conditions. The red trace (squares) is the sensor response for upward flows. The blue trace (diamonds) is the sensor response for downward flows. The yellow trace (triangles) is the temperature difference between upward and downward flow values. 98
Figure 47 Calculation of drainage flux from ADC '*counts*' and 'temperature counts' of Figure 50. (Bond and Hutchinson 2006). *A*, *B*, *C* and *D* are calibration-derived coefficients. 100
Figure 48 The 'tube tensiometer' drainage meter is shown on the left of the figure; the electronics of Figure 50 is incorporated into the base of this device. The detail of the sensing tip can be seen on the right, with the single (white) SDI-12 cable for data and command interchange leaving the instrument for the soil surface. The black vent tubes are needed to allow gauge pressure measurements for depth recording and to allow air trapped in internal pore spaces to vent to atmosphere as air enters the drainage meter. (Bond and Hutchinson 2006) 101
Figure 49 The tube tensiometer drainage meter is inserted down an augured hole several meters deep. The two sensor 'tips' of highly conductive diatomaceous earth are formed in-situ to connect the drainage meter to the soil profile. (Bond and Hutchinson 2006) 102
Figure 50 Multi-channel SVFC ADC with temperature correction, used for 15-bit pressure/depth measurements in the CSIRO 'drainage meter', which consists of twin tube tensiometers incorporating electronic gauge-pressure transducers P1 and P2 to monitor a 0-1m water head in each tube. 102
Figure 51 The CSIRO disc permeameter (Perroux and White 1989) for the measurement of tension-infiltration rate into soil. A small negative pressure of a few centimetres of water head is applied to the supply membrane; this prevents water running down wormholes or cracks in the surface (preferential flow), allowing the determination of the soil's unsaturated hydraulic conductivity (matrix flow). 104
Figure 52. An unsaturated flow permeameter for irrigated agricultural soils. Arranging for the device to always overflow creates a constant head pressure ψ_H above the porous plug. The pressure drop across

the porous plug ψ_P (by Darcy's Law) is designed to exceed the positive head pressure ψ_H of free water above the plug. This ensures that water is drawn out of the instrument at a soil moisture tension ψ_S ($=\psi_H - \psi_P$) such that flows only occur in soil micropores rather than in cracks and macropores. 105
Figure 53 Temperature difference signals T_S-T_F versus velocity for four different power levels. Note that data recording actually begins at $t=0$ on the right-hand side of the plot (off-scale) when flow is at a maximum. The null-points are clearly shown for the higher velocities and higher power levels, but become increasingly indistinct at lower flows. The extra peaks at higher velocities around 1.8 mm/s result from initial thermal stratification of the water column above the sensor and correspond to a shift in the background temperature as the thermocline passes over the sensor. Legend colours are: Red: 97 mW, Blue: 77 mW, Yellow: 62 mW and Green: 48 mW 107
Figure 54. Flow response at constant power (97 mW) with normalised T_S; this small offset change is justified as T_S is arbitrarily chosen anyway with this method. If the theory was correct and the calibration rig working as expected all of these 'minima' should occur at the same velocity at this fixed power level. This is clearly not the case here, although many more weeks were to pass before the cause of this flow instability was discovered. 109
Figure 55. Flow response at constant power (97 mW) with 'normalised' TS and velocity. This allows the 'shape' of the response to be seen over 11 consecutive runs. These plots suggest that the inverted thermal plume is less stable when forced below the thermistor tip by overwhelming flows (to the right of the null-point) in comparison to more stable buoyant plume above the sensor tip (to the left of the null-point). The reasons for the double minima in run 11 (brown trace) and blurred minima in run 3 (dark blue trace) are unknown. 109
Figure 56 Future work: In concept, multiple doughnut-shaped salinity and temperature sensors for monitoring density stratification in estuarine river environments slide down the (looped and electrically insulated) mooring cable to the required depth. Such sensors can be pre-calibrated without first having to be assembled into waterproof strings. The mooring cable forms a single winding for the differential phase shift keyed (PSK) magnetic modem that transfers power to multiple sensors and allows bi-directional flow of measurement commands and data. Bio-film build up is ameliorated by exposure of the electrodes to UV LED radiation inside the measurement cell. Water is pumped through the cell using a thermal pump between measurement cycles. 116
Figure 57. Evidence of 'seiching' in the Torrens Lake during a lake-flushing exercise. The inflow hit the dam wall, creating reflections 133
Figure 58. Evidence of 'sensor calibration consistency' in a 16m-water column. Data prior to sunrise on the 28th May 2003 indicated that the top 14m of the water column mixed to within 0.02°C, vindicating the level of matching (±0.01°C) attained during design and calibration. Systems deployed in the Murray River in June 2009 demonstrated matching over similar depths to within ±0.004°C 133
Figure 59. A 'turn-over' event in early autumn at the White Swan Reservoir in Ballarat Victoria. The bottom 2m of the water column is over 1°C cooler than the 14m water column above it. As the surface layers cool, their density increases and the water column becomes unstable, leading to complete mixing around dawn on the 30th May 2003. 134
Figure 60. Evidence of a cold-water in-rush event from the catchment 'short-circuiting' the Happy Valley Reservoir by under-flowing the main water body. The 'curtain effect' of cooler waters at depth can be seen in the data on the sensors between 25m and 32m from midday on the 8th May 2005, reaching a peak around midnight on the 11th May 2005. 134
Figure 61 A radio-linked ship-to-shore buoy supporting a SDI-12 thermistor string. No data logging occurs on the buoy; instead, all data is transmitted immediately after each 15-minute measurement. 135
Figure 62 This Sealite buoy supports a full logging system, an integrated weather station capsule (Vaisala WXT-510) for air temperature, relative humidity, (drum-head) rainfall sensor, barometric pressure, ultrasonic wind speed and direction and separate global solar and net radiation sensors. All of these sensors are SDI-12 compatible, as is the electronic compass (seen through the instrument door) developed to give a local reference direction for the wind direction sensor. The data logger reads only SDI-12 sensors, and includes Next-G cellular-phone telemetry for remote data collection. 135
Figure 63 A spar-buoy supporting three separate thermistor strings having different anchoring arrangements to allow stratification monitoring in the epilimnion (surface layer), metalimnion (thermocline layer) and hypolimnion (bottom layer) of a reservoir, no matter how the water level changes. The perforated plate at the bottom of the buoy acts as a hydraulic damper to prevent the buoy 'bobbing' in rough water. The length of the chain wrapped around this damper plate is adjusted to change the flotation depth of the spar buoy, which sits low in the water (bottom, right) to allow correct operation of the net radiometer. The latter is part of the weather station cluster mounted on the buoy to monitor wind and solar energy. The station uses cellular phone long-haul telemetry and VHF ship-to-shore SCADA radio systems. 136
Figure 64 Comparison of natural (ln), binary (bln) and simple (sln) logarithms 141
Figure 65 Residual errors between real natural logarithms and the 'Simple log' binary approximation 144
Figure 66 Temperature errors resulting from use of the Simple equation in the first order R-T curve 145

Statement

This work contains no material that has been accepted for the award of any other degree or diploma in any university or other tertiary institution. To the best of my knowledge and belief, this thesis contains no materials previously published or written by another person, except where due reference is made in the text.

I give consent to this copy of my thesis, when deposited in the University library, being available for loan and photocopying, subject to the provisions of the Copyright Act 1968.

The author acknowledges that copyright of published works contained within this thesis (as listed on page 9 of this thesis) resides with the copyright holder(s) of those works.

I also give permission for the digital version of my thesis to be made available on the web, via the University's digital research repository, the Library catalogue, the Australasian Digital Theses Program (ADTP) and also through web search engines, unless permission as been granted by the University to restrict access for a period of time.

……..……..

Andrew John Skinner

Dated: -

Acknowledgments

That this thesis was possible at all owes much to my wife, Claudia. She was unfailingly supportive of a husband plodding through life under the combined stresses that a part-time doctorate added to the already volatile mix of running an engineering business full-time, community responsibilities, home renovations, a large vegetable garden, a family, ageing parents and her own studies and small business start-up. She has my special thanks and love.

I owe a particular debt of gratitude to my thesis supervisor, Professor Martin Lambert, as I shall explain.

There are no schools of 'measurement engineering' within modern universities. This is not surprising, as sensors and measurements are common to all the physical sciences, and their design requires input from the disciplines of physics, sensors, electronics, mechanics, software and firmware plus specialist fields such as fluid dynamics, limnology, meteorology and so forth. It made no sense to me to undertake a PhD degree in the electronic and electrical engineering schools where I had received previous Bachelor and Master's degrees, and in a field in which I already had a considerable amount of industrial experience in Australia, Papua-New Guinea and Canada. Rather, it seemed to me to be appropriate to seek a PhD supervisor in the area of water engineering where I could receive specialised supervision in the arcane art of fluid and thermal dynamics – areas in which I had no training or expertise, but which were critical to the perfection of a thermal sensor that would attempt to create a new 'slow flow' measurement record in the field of environmental engineering. I will be forever grateful to Martin for taking on the considerable risk of supervising an unknown student having such a tenuous connection to his own field of water engineering. I have never been disappointed in that decision. That a number of working instruments and original IEEE journal papers have come out of this PhD program owes much to Martin's patience, rigour and consistency and his willingness to accept the slow pace at which I was able to proceed.

My business partner, Joe Hoogland (and Managing Director of our company 'Measurement Engineering Australia'), put up with raids on the company's resources and my sometimes-distracted attention span. He was able to see the (very long) picture of having an Engineering Director who would one day understand the academic system at first hand and be trained in the rigours of research in that parallel universe.

Along the journey I had access to some very fine engineers working in the commercial arena, and some fine scientists who worked for the CSIRO. They let me pick

their brains, and expressed enthusiasm for my sometimes-quaint ideas. In particular, Dr Allan Wallace of Avocet Consulting in Adelaide South Australia provided invaluable CFD modeling in support of the experimental work, help with fluid dynamic concepts such as the Hagen-Poiseuille theory for the seepage meter and co-authorship on the 5th paper (Chapter 7) that supported my (then) vague ideas about a null-buoyancy flow meter principle.

Finally, there is a bunch of folk I don't know - the dozen or so reviewers and editors who read my prototype papers and offered ways to improve them. They contributed immeasurably to the quality of the final papers and hence to this thesis.

Abstract

Measurement of very slow flows in environmental engineering

Many of the flow metering techniques used in industrial applications have finite limits at slow fluid velocities in the order of 10 mm/s. By comparison, many environmental flow rates occur two or more orders of magnitude below this, examples being the rate of sap flow in plants, the percolation rate of rainfall into soil and through the landscape, flows in the benthic boundary layer of lakes, the movement of water through sandy river banks or in the swash zone of beaches, or the seepage rate of groundwater into river beds.

Unlike well-defined industrial flow measurement systems, nature is extravagant with her variability. To counter this, sensor systems in environmental engineering have to be widely flung, inexpensive and highly matched. 'Smart' sensors must therefore be simple designs having calibration techniques that can be highly automated. Additionally, such sensors must be able to compute real data locally, apply temperature corrections, compensate for inherent non-linearity and integrate without fuss into environmental logging systems. This thesis describes the development of sensors and experimental techniques in five very slow flow rate applications in environmental engineering via three published papers and two papers in submission: -

[1]Gravitational flows in a large stratified water body were identified using smart temperature strings; these sensors demonstrated new techniques for low-cost but high-precision thermistor temperature measurements, sensor temperature matching, the generation of complex algorithms within a simple sensor and a method for obtaining two-point calibrations for non-linear sensors. Field work with these sensor strings identified 'short-circuiting' of an urban reservoir during a storm event over the catchment which led to denser cold-water inflows moving along the bottom boundary layer of the lake.

[2]The movement of 'wetting fronts' in the soil below plants mobilizes toxic salts left behind in the soil profile by crop evapotranspiration processes that take up only fresh water. These problems are exacerbated in semi-arid areas under crops irrigated with

[1] Skinner, A.J. and Lambert, M.F. (2006). 'Using smart sensor strings for continuous monitoring of temperature stratification in large water bodies.' IEEE Sensors, Vol. 6, No. 6, December 2006

[2] Skinner, A.J. and Lambert, M.F. (2009). 'An automatic soil salinity sensor based on a wetting front detector.' IEEE Sensors, in submission, July 2009

brackish water. Automatic recording of soil salinity levels is possible using an instrument based on the combination of an EC (electrical conductivity) sensor with a platinum resistance temperature sensor within a funnel-shaped 'wetting front detector' buried in the soil. These two combined sensors extend the usage of the low-cost 16-bit charge-balance analog-to-digital converter developed for use in stratification measurements.

[3]Measurement of sap flow in irrigated agriculture for determining when to irrigate crops was found to be of limited use for determining 'when to water' because the flow signal is masked by the plant's genetically-coded regulatory systems. A new 'double bridge' analog control circuit for a self-heating thermistor was designed and described as a thermal diffusion sensor to study plant water status and the onset of irrigation stress in grapevines once sap flow had ceased. A laboratory experiment on a cut vine cane demonstrated that this thermal diffusion sensor was sensitive enough to track the response of the living cane to external forcing events that changed its plant water status.

[4]The same double-bridge thermistor control circuit was used to investigate the lower limits of very slow ***upward*** flow measurement for use in the funnels of automatic seepage meters designed to monitor groundwater flows into the bottom of rivers and lakes. Theoretical, CFD (computational fluid dynamics) and two different experimental studies showed that flows between 0.03 mm/s and 3 mm/s could be measured in the presence of buoyant thermal plumes from the self-heated spherical sensor in free water.

[5]A new type of null-buoyancy thermal flow sensor is described; it is designed specifically for the measurement of ***downward*** flows below 3 mm/s using a single thermistor. A typical application of such flow meter technology would be in the measurement of the hydraulic conductivity of soil to determine the rate at which rainfall can enter the landscape without run-off and erosion. The thermistor power dissipation is adjusted so that the upward thrust of the buoyant thermal plume from the warm thermistor sensor exactly counter-balances the downward bulk fluid velocity, resulting in flow stagnation at the sensor tip characterized by a corresponding local peak in the sensor's

[3] Skinner, A.J. and Lambert, M.F. (2009). 'A log-antilog analog control circuit for constant-power warm-thermistor sensors – Application to plant water status measurement.' IEEE Sensors, Vol. 9, Issue 9, September 2009

[4] Skinner, A.J. and Lambert, M.F. (2009). 'Evaluation of a warm-thermistor flow sensor for use in automatic seepage meters.' IEEE Sensors, Vol. 9, Issue 9, September 2009

[5] Skinner, A.J. and Lambert, M.F. (2009). 'A null-buoyancy thermal flow meter: Application to the measurement of the hydraulic conductivity of soils.' IEEE Sensors, in submission, August 2009.

temperature response. Power dissipation must increase with the square of an increasing flow velocity to maintain this null-point.